

# Change Diffusion: Change Detection Map Generation Based on Difference-Feature Guided DDPM

Yihan Wen, Jialu Sui, Xianping Ma, Wendi Liang, Xiaokang Zhang, Man-On Pun

**Abstract**—Deep learning (DL) approaches based on CNN-purely or Transformer networks have demonstrated promising results in bitemporal change detection (CD). However, their performance is limited by insufficient contextual information aggregation, as they struggle to fully capture the implicit contextual dependency relationships among feature maps at different levels. Additionally, researchers have utilized pre-trained denoising diffusion probabilistic models (DDPMs) for training lightweight CD classifiers. Nevertheless, training a DDPM to generate intricately detailed, multi-channel remote sensing images requires months of training time and a substantial volume of unlabeled remote sensing datasets, making it significantly more complex than generating a single-channel change map. To overcome these challenges, we propose a novel end-to-end DDPM-based model architecture called change-aware diffusion model (CADM), which can be trained using a limited annotated dataset quickly. Furthermore, we introduce dynamic difference conditional encoding to enhance step-wise regional attention in DDPM for bitemporal images in CD datasets. This method establishes state-adaptive conditions for each sampling step, emphasizing two main innovative points of our model: 1) its end-to-end nature and 2) difference conditional encoding. We evaluate CADM on four remote sensing CD tasks with different ground scenarios, including CDD, WHU, Levier, and GVL. Experimental results demonstrate that CADM significantly outperforms state-of-the-art methods, indicating the generalization and effectiveness of the proposed model.

**Index Terms**—Denoising diffusion probabilistic model, Change detection, generative models

## I. INTRODUCTION

Change detection (CD) from multitemporal remote sensing imagery has obtained significant attention in remote sensing research, specifically in the field of land resource surveillance, natural hazard evaluation, and ecosystem observation [1] [2] [3]. Over the years, various CD techniques have been developed, falling into categories such as image algebra, image

This work was supported in part by the National Key R&D Program of China under grant 2018YFB1800800, the Basic Research Project under Grant HZQB-KCZYZ-2021067 of Hetao Shenzhen-HK S&T Cooperation Zone, Shenzhen Outstanding Talents Training Fund 202002, Guangdong Research Projects under Grant 2017ZT07X152 and 2019CX01X104, the Guangdong Provincial Key Laboratory of Future Networks of Intelligence under Grant 2022B1212010001, the National Natural Science Foundation of China under Grant 41801323. (Corresponding authors: Man-On Pun; Xiaokang Zhang)

Yihan Wen, Xianping Ma, Jialu Sui and Man-On Pun are with the School of Science and Engineering, The Chinese University of Hong Kong, Shenzhen, China (e-mail: wenyihan4396@gmail.com; xianpingma@link.cuhk.edu.cn; jialusui@link.cuhk.edu.cn; SimonPun@cuhk.edu.cn).

Xiaokang Zhang is with the School of Information Science and Engineering, Wuhan University of Science and Technology, Wuhan 430081, China (e-mail: natezhangxk@gmail.com).

transformation, and machine learning approaches. Image algebra methods involve techniques like image differencing [4] and change vector analysis (CVA) [5, 6] to extract change magnitudes. Meanwhile, image transformation techniques such as principal component analysis [7] and histogram [8] trend similarity aim to amplify change information. In recent years, machine learning-based methods have gained attention, focusing on pixel classification as changed or unchanged. To improve the robustness of machine learning algorithms, considerable efforts have been dedicated to dimensionality reduction, feature extraction, and optimization processes. These advancements have contributed to the development of CD techniques.

In the early stages of deep learning-based CD, deep neural networks [9–12] were typically utilized to extract distinguishable features between bitemporal images. Such networks are primarily composed of multiple layers of CNN convolutional networks and residual operations, which directly extract features from input images. For example, Zhan et al. [13] employed Siamese CNN to extract deep features that are more abstract and robust compared to handcrafted features. In addition, Daudt et al. [14] proposed a Fully Convolutional Neural Network (FCNN) with Unet architecture, which further enhances the accuracy of CD by extracting multi-scale feature information. Despite the improvements in metrics such as F1 and IoU, these methods suffer from the loss of accurate spatial position information due to the successive downsampling operations during the convolution process. To address this issue, Sheng et al. [15] proposed the SNUNet-CD architecture consisting of a siamese network and NestedUNet to preserve coarse-grained semantic information. However, the spatial-temporal information utilized by the DNN-based methods is very limited due to the small image patches. To further enhance the performance of CD, attention mechanisms have been employed to refine features and achieve superior feature representations, encompassing spatial and channel attention in [16–19], self-attention in [20], dual attention in [21], among others. Notably, Zhang et al. [16] leveraged attention modules within the difference discrimination network to efficiently merge deep features of raw images with image difference features, thereby facilitating change map reconstruction. Furthermore, Hao et al. [20] introduced a self-attention mechanism for CD, which captures abundant spatiotemporal relationships to obtain illumination-invariant and more robust features. In addition, a dual attentive fully convolutional Siamese networks (DASNet) framework [21] has been proposed to extract satisfactory

features capable of effectively distinguishing between changed and unchanged areas. Additionally, in contrast to DNN-based models, the Transformer structure has shown promising performance in several computer vision tasks, including CD [22–25], by overcoming the limitations of capturing long-range dependencies. The self-attention modules introduced by the Transformer capture global interactions between contexts and address the limitation of the receptive field in CNN-based models. However, attention-based methods may suffer from increased computational complexity, the need for finetuning which could pose challenges in certain applications or scenarios.

Furthermore, the introduction of Denoising Diffusion Probabilistic Models (DDPM) has significantly enhanced the generative capabilities of diffusion model, surpassing the performance of Generative Adversarial Networks (GANs) and transformers. Consequently, DDPM has been increasingly employed in various domains, including super-resolution [26], segmentation [27–29], inpainting [30], and conditional image generation [31, 32]. In [33], DDPM is employed as a feature extractor to capture the semantic information. Specifically, a diffusion model can be trained via a variational inference procedure on an extensive collection of off-the-shelf remote sensing images to generate images, to generate images that increasingly resemble authentic images over a finite time period. Throughout this training process, the diffusion model progressively acquires a potent semantic extraction capability, which is instrumental in acquiring a CD map. However, the previous DDPM methods did not specifically focus on generating a single-channel CD map. Instead, their primary objective was to train a model capable of generating intricately detailed, multi-channel remote sensing images that closely resemble real-world scenes. Accomplishing this task necessitates months of training time and a substantial volume of unlabeled remote sensing datasets. The complexity of this endeavor is significantly higher compared to the generation of a single-channel change map.

In contrast, this paper proposes a novel approach by designing a DDPM-based model architecture called RS-CADM, which can be trained end-to-end using a limited annotated dataset quickly. The end-to-end properties of RS-CADM make it well-suited for single-classification tasks such as generating CD maps.

RS-CADM offers several advantages for accurate CD map generation. Firstly, the diffusion model in RS-CADM employs probabilistic modeling to capture the diversity and complexity of input images, establishing intricate data distribution models [33]. This enables the model to adapt to various scenes and image features, including the shape, size, and texture of objects. Additionally, the diffusion model in RS-CADM leverages its ability to capture long-range dependencies in the data by considering the spatial and temporal relationships among pixels in the input images [34]. This understanding of contextual information and capture of global dependencies is particularly advantageous for CD tasks involving large areas and complex spatial patterns. Furthermore, the diffusion model is trained using variational inference [35], a powerful and flexible technique for learning complex probabilistic models.

This training procedure, combined with the end-to-end training approach of RS-CADM, enables the model to gradually learn and refine its representation of the data, resulting in improved generation accuracy of CD maps.

Moreover, in remote sensing CD tasks, distinguishing subtle and irregular buildings or natural scenes from the background can be challenging and ambiguous. To address this, RS-CADM incorporates an adaptive calibration process, utilizing dynamic conditional encoding over vanilla DPM. During the iterative sampling process, RS-CADM conditions each step using bitemporal images before learning the CD map. Additionally, a noise suppression-based semantic enhancer is employed to suppress high-frequency noise and incorporate the CD map from the current step into the pre-change image and post-change image at each iteration, enhancing the differential information. Finally, the computation of the difference between multi-level features from the pre-change image and the post-change image further improves the generation accuracy of the change map.

In summary, the main contributions of this study are the design of the RS-CADM model, which leverages DDPM and incorporates adaptive calibration and noise suppression-based enhancement techniques. These contributions enable RS-CADM to generate highly accurate CD maps, making it a promising approach for remote sensing CD tasks.

- 1) Instead of leveraging an extensive collection of off-the-shelf remote sensing images to train an encoder, We propose RS-CADM, an end-to-end DDPM architecture, which directly generates CD maps. The training process utilizes variational inference [30], a powerful and flexible technique for learning complex probabilistic models, facilitating the gradual learning and refinement of the model's data representation, enabling to effectively distinguish subtle and irregular buildings or natural scenes from the background.
- 2) An adaptive calibration conditional difference encoding over DDPM is proposed to archive a precise CD map. This method involves computing the difference between multi-level features extracted from the pre-change image and the post-change image during the iterative sampling process. This difference is then utilized to guide the sampling process for generating the CD map.
- 3) We employ a noise suppression-based semantic enhancer (NSSE) to treat the CD information from the current step as prior knowledge. The NSSE utilizes an attentive-like mechanism to suppress high-frequency noise in the CD information. Subsequently, this prior knowledge is integrated into the difference features during the conditional encoding process at each iteration. This approach enhances the differential information and ultimately improves the quality of the CD map.

The rest of this paper is organized as follows. Section II describes the related work of deep learning-based CD methods and the recent DDPM-based models in RS. Section III gives the details of our proposed method. Extensive experimental results are reported in section IV. The discussion is given in section V.

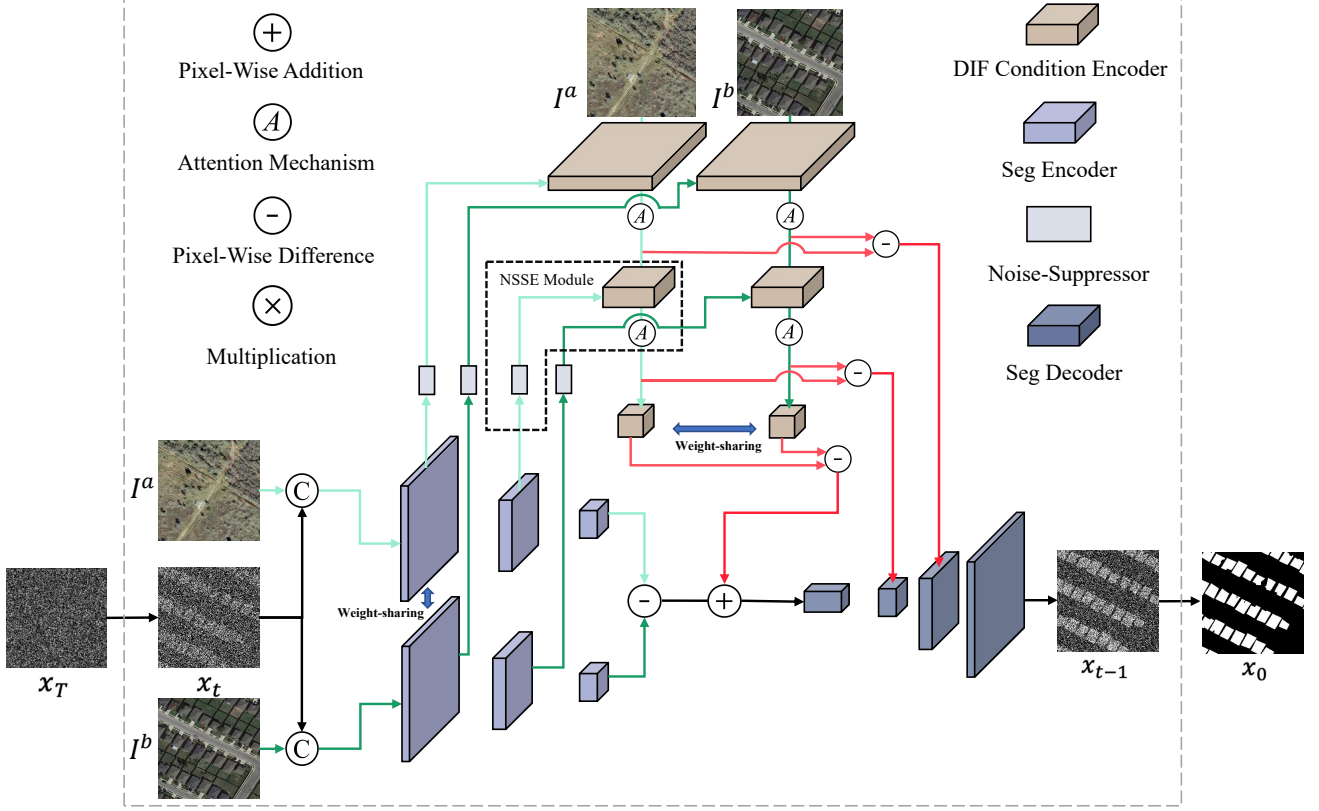


Fig. 1. An illustration of one timestep with the proposed RS-CADM. For clarity, the feature flows in Segmentation Encoder (Seg Encoder) blocks and in Segmentation Decoder (Seg Decoder) blocks are omitted.

## II. RELATED WORK

### A. CNN-based models

In the early stages of CD, CNN-based models were widely used for extracting difference maps and features, primarily focusing on capturing local spatial information [36–38]. For example, a symmetric convolutional coupling network called SCCN [39] employed unsupervised learning to optimize a coupling function based on heterogeneous images. It aimed to capture the intrinsic relationship and highlight the differences between the input images. Additionally, skip-connections were introduced in models like ReCNN [40] to handle temporal connections in multitemporal data and extract rich spectral-spatial features. However, CNN-based methods have inherent limitations in modeling global dependencies and capturing comprehensive spatial-temporal information. These models are primarily focused on local regions and lack the ability to capture long-range relationships across the entire image. Therefore, CNN-based approaches may struggle to capture complex patterns and changes that occur over larger areas or have intricate spatial distributions.

### B. Transformer-based models

In comparison to CNN-based models, the Transformer architecture has demonstrated exceptional performance in various computer vision tasks, including CD, by effectively addressing the challenge of capturing long-range dependencies [41, 42]. The use of self-attention modules in Transformers

enables the capturing of global contextual relationships, which helps overcome the receptive field limitations observed in CNN-based models. Several studies have built upon this success by introducing Transformer-based models tailored for CD. For example, SwinsUNet [43] introduced a pure Transformer network with a Siamese U-shaped structure, leveraging the Swin Transformer block for the encoder, fusion, and decoder components. Similarly, BCL [44] proposed a self-attention mechanism in the feature extraction process to enhance the performance of CD methods by exploring relationships among spatial-temporal pixels. However, despite their advantages, Transformer-based models have certain limitations. One notable drawback is that these models often struggle to accurately predict the fine-grained details of CD maps. This limitation arises from the inherent characteristics of Transformers, which can lead to relatively low precision and coarse estimation of the edge details in the predicted CD maps. While Transformers excel at capturing global contextual information, they may not be as effective in capturing intricate local variations and edge details. This limitation hinders their ability to precisely delineate the boundaries of change regions and may result in less refined predictions.

### C. DDPM-based models

Compared to CNNs and Transformers, DDPM-based generative models offer several advantages that enable them to capture complex data distributions and accurately predict fine-grained details and edge information in CD maps. Firstly, the

diffusion model employed in RS-CADM leverages probabilistic modeling to capture the diversity and complexity of input images. By learning to transform a standard normal distribution into an empirical data distribution, the model can adapt to various scenes and image features, including the shape, size, and texture of objects. This capability allows DDPM-based models to precisely delineate the boundaries of change regions and generate CD maps with refined predictions. Bandara et al. [34] first applied the DDPM to remote sensing CD task, which utilized a pre-trained DDPM as an encoder to assist feature extraction. At the same time, it did not fully leverage the advantages of DDPM and suffered from high training costs. To overcome this limitation, we incorporate DDPM directly into the CD framework, allowing the model to learn both feature representations and the probability distribution of the data simultaneously. Our model significantly reduces training costs as well as improves the accuracy of CD models.

### III. METHODOLOGY

#### A. CADM

The diffusion model is a generative model consisting of two stages, namely, the forward diffusion stage and the backward diffusion stage. In the forward process, the segmentation label  $x_0$  is gradually added with Gaussian noise through a series of steps  $T$ . During the backward diffusion stage, a neural network is trained as a noise predictor to reverse the noising process and recover the original data.

1) *Forward Process*: The Diffusion process involves generating a series of data points  $x_1, x_2, \dots, x_T$ , conditioned on a given initial data distribution  $x_0 \sim q(x_0)$ . This process can be mathematically formulated as follows:

$$q(x_1, \dots, x_T | x_0) = \prod_{i=1}^n q(x_t | x_{t-1}) \quad (1)$$

$$q(x_t | x_{t-1}) = \mathcal{N}(x_t; \sqrt{1 - \beta_t} x_{t-1}, \beta_t I), \quad (2)$$

where  $\{\beta_1, \dots, \beta_T\} \in (0, 1)$  is a variance schedule consisting of a set of hyperparameters. With this recursive formula, we establish the mathematical relationship between  $x_0$  to  $x_t$ , which can be formulated as:

$$x_t = \sqrt{\bar{\alpha}_t} x_0 + \sqrt{1 - \bar{\alpha}_t} \epsilon. \quad (3)$$

2) *Reverse Process*: the reverse process involves transforming the latent variable distribution  $p_\theta(x_T)$  into the data distribution  $p_\theta(x_0)$ , which is parameterized by  $\theta$ . This transformation is defined by a Markov chain featuring learned Gaussian transitions, with the initial distribution  $p(x_T)$  represented as a standard normal distribution  $p(x_T) = \mathcal{N}(x_T; 0, I)$  :

$$p_\theta(x_0, \dots, x_{T-1} | x_T) := \prod_{t=1}^T p_\theta(x_{t-1} | x_t), \quad (4)$$

$$p_\theta(x_{t-1} | x_t) := \mathcal{N}(x_{t-1}; \mu_\theta(x_t, t), \sigma_\theta^2(x_t, t) I), \quad (5)$$

where  $\theta$  denotes the parameters of the reverse process. To maintain symmetry with the forward process, the noise image is iteratively reconstructed through the reverse process until a final clear segmentation is achieved.

3) *Noise Predictor*: In accordance with the standard implementation of DDPM, we employ a UNet as a noise predictor. An illustration is shown in Figure 1. In order to achieve the CD map directly, we condition the step estimation function by raw images prior, which can be represented as:

$$\epsilon_\theta(x_t, I_a, I_b, t) = D((E_t^{I_b} - E_t^{I_a}) + (E_t^{x \odot I_a} - E_t^{x \odot I_b}), t), \quad (6)$$

where  $E_t^{I_b} - E_t^{I_a}$  is the conditional difference embedding feature, in our case, the bitemporal images embedding feature,  $E_t^{x \odot I_a} - E_t^{x \odot I_b}$  is the CD map embedding feature of the current step. The two components are added and sent to the Seg Decoder  $D$  for reconstruction. The step-index  $t$  is integrated with the added embedding and decoder features.

#### B. Noise Predictor

In remote sensing, previous researchers have commonly used DDPM as a feature extractor for obtaining multidimensional features. The objective of this training process is to acquire a model capable of generating intricately detailed, multi-channel remote sensing images that closely resemble real-world scenes. Although this approach has improved accuracy to some extent, accomplishing this task necessitates months of training time and a substantial volume of unlabeled remote sensing datasets. The complexity of this endeavor is significantly higher compared to the generation of a single-channel change map.

In contrast to previous methods, the proposed model's significant advantage lies in its ability to generate high-quality CD maps directly through end-to-end training without the need for additional training of diffusion models.

1) *Difference Conditional Encoding*: We proposed a creative Encoding approach called Difference Conditional Encoding to provide change information for each sampling of the diffusion model.

The pre-change  $I_a$  and post-change  $I_b$  images contain accurate segmentation target information but discriminating change information between them can be difficult. On the other hand, the current-step CD map contains enhanced target regions but with a reduced level of accuracy. Drawing inspiration from these situations, we integrate the current-step CD map's information  $x_t$  into the difference conditional encoding for the mutual complement. Specifically, we leverage the conditional encoder to extract each hierarchical level of the conditional feature maps from pre-change image  $I_a$  and post-change image  $I_b$ , respectively.

Furthermore, the extracted multi-level information from the condition encoder is integrated with the current-step segmentation information  $x_t$  for the mutual complement. Each scale of the conditional feature map  $m_a^k \in R^{C/2 \times H \times W}$  and  $m_b^k \in R^{C/2 \times H \times W}$  are respectively fused with the  $x_t$  encoding features  $m_{x_t \odot a}^k \in R^{C \times H \times W}$ , and  $m_{x_t \odot b}^k \in R^{C \times H \times W}$  with the same shape,  $k$  is the index of the layer. The fusion is implemented by Noise suppression-based semantic enhancer (NSSE) with an attentive-like mechanism.

$$NSSE(m_a^k, m_{x_t \odot a}^k) = LN(m_a^k) \otimes A(LN(m_{x_t \odot a}^k)) \quad (7)$$

$$NSSE(m_b^k, m_{x_t \odot b}^k) = LN(m_b^k) \otimes A(LN(m_{x_t \odot b}^k)), \quad (8)$$

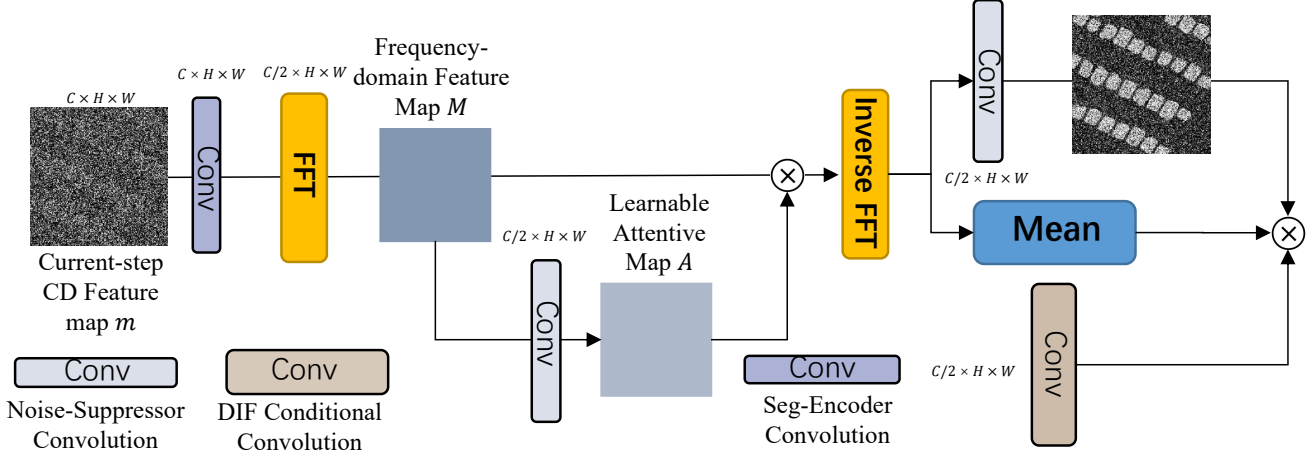


Fig. 2. An illustration of an Attentive module called NSSE. FFT denotes Fast Fourier Transform (FFT). We employ the Fast Fourier Transform (FFT) to convert image information into the frequency domain, where an attentive-like mechanism is utilized to suppress high-frequency information. This process helps to extract CD information, which is then transformed back into image information using the Inverse Fast Fourier Transform (IFFT).

in which, the symbol  $\otimes$  denotes element-wise multiplication, the abbreviation  $LN$  represents the technique of layer normalization. Additionally,  $A$  represents an attentive-like module that consists of a noise suppressor (a learnable version of frequency filters) and attention mechanisms in both channel and pixel-wise dimensions. Finally, the change information is computed by the pixel-wise difference operation between enhanced multi-scale features of  $I_a$  and  $I_b$ , which is formulated as:

$$Diff(m_a^k, m_b^k, m_{x_t}^k) = NSSE(m_b^k, m_{x_t \odot b}^k) - NSSE(m_a^k, m_{x_t \odot a}^k) \quad (9)$$

This operation is carried out within the middle two stages, with each stage comprising convolutional layers designed based on the ResNet34 architecture. This approach allows the RS-CADM model to localize and fine-tune the segmentation process dynamically.

### C. Network Details

The RS-CADM primarily consists of two key components: a U-Net network, which functions as a noise predictor to effectively estimate noise related to difference feature representations, and a novel Difference Conditional Encoding mechanism that seamlessly embeds difference information derived from pre-change and post-change images, thereby substantially enhancing CD performance.

To fully leverage the multi-step iterative prediction capability of the diffusion model, we propose a noise suppression-based semantic enhancer (NSSE) to integrate the current-step CD feature information into the conditional encoding, enhancing the CD information extracted by the Conditional Encoding. Furthermore, the multi-scale CD feature maps extracted by the encoder will be fused back to the U-Net model through skip connections and pixel-wise addition operations to locate the semantic regions of the CD accurately.

In the following two sections, we will delve into the details of the NSSE and the CD localization operations built upon the ResNet architecture. These components play a crucial role

in our proposed method's ability to effectively and accurately detect changes in remote sensing imagery.

1) *NSSE*: We incorporate a noise suppression module [45] into the feature integration pathways, with the objective of suppressing noise-related components inherent in the  $x_t$  features. The central idea involves mapping  $x_t$  to the frequency domain and eliminating high-frequency noise of  $x_t$  by learning a parameterized attention (weight) map within this domain. Given an  $x_t$  encoder feature map,  $m_{x_t \odot Img}^k \in R^{C \times H \times W}$ ,  $Img = a, b$ , we initially perform a 2D FFT (Fast Fourier transform) along the spatial dimensions, formulated as

$$M_{x_t \odot Img}^k \in C^{\frac{C}{2} \times H \times W} = FFT(Conv(m_{x_t \odot Img}^k)), \quad (10)$$

where  $FFT(\cdot)$  represents the 2D FFT. We then modulate the spectrum of  $m$  by multiplying a parameterized attentive map  $A_{x_t \odot Img}^k \in \frac{C}{2}^{H \times W \times C}$  to  $M$ :

$$M_{x_t \odot Img}^k \in C^{\frac{C}{2} \times H \times W} = A_{x_t \odot Img}^k \otimes M_{x_t \odot Img}^k, \quad (11)$$

where  $\otimes$  denotes the element-wise product. Lastly, we convert  $M_{x_t \odot Img}^k$  back to the spatial domain using the inverse FFT:

$$m'_{x_t \odot Img}^k \in C^{\frac{C}{2} \times H \times W} = F^{-1}(M_{x_t \odot Img}^k). \quad (12)$$

The noise suppression module can be considered a learnable version of frequency filters, which are widely applied in digital image processing [46]. Unlike spatial attention, it globally adjusts the components of specific frequencies, enabling it to learn to constrain the high-frequency component for adaptive integration.

Moreover, pixel-wise and channel-wise attention mechanisms are employed to facilitate the fusion process between  $m'$  and bitemporal images, as illustrated in Figure A. Specifically, CD feature  $m'_{x_t \odot Img}^k \in C^{\frac{C}{2} \times H \times W}$  extracted from  $x_t$  is fed into two separate convolution layers.

$$M_{pixelwise}^{Img, Img=a,b} = Conv(LN(m'_{x_t \odot Img}^k)), \quad (13)$$

$$M_{channel}^{Img, Img=a,b} = Mean(LN(m'_{x_t \odot Img}^k)), \quad (14)$$

where Conv maps  $m_{x_t \odot \text{Img}}^{k'} \in R^{\frac{C}{2} \times H \times W}$  to a feature map  $M_{\text{pixelwise}}^{\text{Img}, \text{Img}=a, b} \in R^{1 \times H \times W}$  with a single channel, serving as a trainable pixel-wise filter. Mean represents the global average pooling operation, yielding a one-dimensional vector of length  $C$ , providing channel attention information for  $m_a^k$  ( $m_b^k$ ). The fusion process of this attention mechanism can be formulated as:

$$A(m_a^k, m_{x_t \odot a}^{k'}) = M_{\text{pixelwise}}^{\text{Img}=a} \otimes M_{\text{channel}}^{\text{Img}=a} \otimes M(\text{LN}(m_a^k)) \quad (15)$$

$$A(m_b^k, m_{x_t \odot b}^{k'}) = M_{\text{pixelwise}}^{\text{Img}=b} \otimes M_{\text{channel}}^{\text{Img}=b} \otimes M(\text{LN}(m_b^k)). \quad (16)$$

Furthermore, we incorporate the pixel-wise difference to merge the multi-scale feature maps of the semantically enhanced bitemporal images:

$$Dif(m_a^k, m_b^k, m_{x_t \odot a}^{k'}, m_{x_t \odot b}^{k'}) = A(m_b^k, m_{x_t \odot b}^{k'}) - A(m_a^k, m_{x_t \odot a}^{k'}) \quad (17)$$

Such a fusion strategy effectively enhances the semantic information of differences between the pre-change image and the post-change image.

2) *ResNet based Seg Encoder and Decoder* : The main architecture of CADM is a modified ResUNet, which we implement with two ResNet encoders following a ResNet decoder.  $I_a$  and  $I_b$  are encoded and fused with differential conditional encoders. Moreover,  $x_t$  is encoded by a ResNet encoder. In the decoder module, Multi-scale change feature maps  $Dif(m_a^k, m_b^k, m_{x_t \odot a}^{k'}, m_{x_t \odot b}^{k'}), k = 0, 1, 2$  containing difference information from conditional encoders and current-step CD features  $m_{x_t \odot a}^{k'} - m_{x_t \odot b}^{k'}, k = 0, 1, 2$  are fused within the convolutional decoder through pixel-wise addition and skip connections as shown in Figure 1. In particular, the difference feature map  $Dif(m_a^k, m_b^k, m_{x_t \odot a}^{k'}, m_{x_t \odot b}^{k'}), k = 2$  and  $m_{x_t \odot a}^{k'} - m_{x_t \odot b}^{k'}, k = 2$  are combined and passed on to the last encoding stage. Subsequently, a decoder with a residual network is employed to decode the high-dimensional features while incorporating the features  $Dif(m_a^k, m_b^k, m_{x_t \odot a}^{k'}, m_{x_t \odot b}^{k'}), k = 0, 1$  through pixel-wise addition into the feature map. By iteratively sampling Gaussian noise 1,000 times, the final CD map is ultimately obtained, providing an accurate representation of the differences observed between the input images.

## IV. EXPERIMENT

### A. Experimental Dataset

We conduct comparative experiments on four CD datasets.

The CDD (CD Dataset) [47] is a publicly available large-scale CD dataset, specifically designed to capture season-varying changes. It consists of 7 pairs of images with a resolution of  $4725 \times 2700$  pixels for manual ground truth creation, 4 season-varying image pairs with minimal changes, and a resolution of  $1900 \times 1000$  pixels for adding additional objects manually. The spatial resolution of the obtained images ranges from 3 to 100 cm/px, allowing the dataset to cover objects of various sizes, from cars to large construction structures, as well as seasonal changes of natural objects, such as single trees and wide forest areas.

The dataset was generated by cropping randomly rotated  $256 \times 256$  fragments ( $0 - 2\pi$ ) with at least a part of the target object. This ensured that object center coordinates were unique, and the distance between object centers for each axis was 32 pixels. The final dataset contains 16,000 image sets with an image size of  $256 \times 256$  pixels: 10,000 training sets and 3,000 test and validation sets.

LEVIR-CD [48] is a public large-scale building CD dataset. It contains 637 pairs of high-resolution (0.5m) RS images of size  $1024 \times 1024$ . We follow its default dataset split (training/validation/test). For the limitation of GPU memory capacity, we cut images into small patches of size  $256 \times 256$  with no overlap. Therefore, we obtain 7120/1024/2048 pairs of patches for training/validation/test, respectively.

WHU-CD [49] is a public building CD dataset. It contains one pair of high-resolution (0.075m) aerial images of size  $2507 \times 15354$ . As no data split solution is provided in [54], we crop the images into small patches of size  $256 \times 256$  with no overlap and randomly split it into three parts: 6096/762/762 for training/validation/test, respectively.

The GVLM (global very-high-resolution landslide mapping) [50] is a publicly available CD dataset specifically designed for monitoring landslide occurrences. It contains 17 pairs of high-resolution landslide images with a resolution of  $4349 \times 4096$  pixels for manual ground truth creation.

The dataset was generated by cropping  $256 \times 256$  fragments with at least a part of the target object. This method ensured the uniqueness of object center coordinates and a distance of 32 pixels between object centers for each axis. The final dataset comprises 7,595 image sets with an image size of  $256 \times 256$  pixels: 6,075 training sets and 760 test and validation sets. This dataset is particularly valuable for developing and evaluating CD algorithms for landslide monitoring and mitigation.

### B. Implementation Details

The RS-CADM model is implemented using the PyTorch framework and trained on a single NVIDIA GeForce RTX 4090 Ti GPU. For data augmentation, we apply a range of standard techniques to the input image patches, including horizontal and vertical flipping, rescaling, random cropping, and Gaussian blurring to enhance the model's generalization capabilities. The model comprises several layers of varying dimensions to effectively capture and process features from the input data. We employ a combination of convolutional, normalization, and activation layers, followed by pooling and fully connected layers in the model architecture. The precise number of layers and dimensions are chosen based on the specific dataset and application requirements to achieve optimal performance. To optimize the model, we utilize stochastic gradient descent (SGD) with momentum as the optimization algorithm. The momentum is set to 0.99, and the weight decay parameter is set to 0.0005. The learning rate is initially set to 0.0001 and is linearly decayed to 0 over the course of 200 epochs. Validation is performed periodically throughout the training process to monitor the model's performance and prevent overfitting. The choice of hyperparameters is determined through extensive experimentation and cross-validation,

ensuring the best possible performance of the RS-CADM model on the target CD tasks.

### C. Evaluation Metrics

The F1-score, Intersection over Union (IoU), and overall accuracy (OA) are common performance metrics used to evaluate the effectiveness of various models, particularly in tasks such as CD and image segmentation. Each of these metrics provides a different perspective on the performance of a model.

We use the F1-score with regard to the change category as the main evaluation indices which is the F1-score is a harmonic mean of precision and recall, offering a balanced assessment of a model's accuracy and completeness. It is calculated as follows:

$$F1 = \frac{2}{recall^{-1} + precision^{-1}}, \quad (18)$$

where *recall* and *precision* can be formulated as:

$$Recall = \frac{TP}{TP + FN} \quad (19)$$

$$Precision = \frac{TP}{TP + FP} \quad (20)$$

Additionally, IoU is a metric used to evaluate the degree of overlap between two sets, typically the predicted segmentation map and the ground truth. In the context of CD, IoU for the change category is calculated as follows:

$$IoU = \frac{TP}{TP + FN + FP}. \quad (21)$$

OA is a measure of the proportion of correctly classified instances out of the total instances. It is calculated as:

$$OA = \frac{(TP + TN)}{(TP + TN + FN + FP)}, \quad (22)$$

where TP, TN, FP, and FN represent the number of true positive, true negative, false positive, and false negative respectively.

### D. Experimental Comparison

We conduct a comprehensive comparison between our proposed approach and several state-of-the-art methods in the field. These methods encompass three convolution-based techniques, namely FC-SC [13], SNUNet [15], and DT-SCN [51], two transformer-based strategies, including BIT [41] and ChangeFormer [42]. This comparative analysis allows us to better understand the relative performance and capabilities of our method in relation to existing approaches within the literature.

FC-Siam-Conc [13] leverage a Siamese FCN to extract multi-level features while employing feature concatenation as a fusion strategy for bitemporal information. SNUNet [15] represents another instance of an FF method called a Multi-scale feature concatenation, which combines the Siamese network and NestedUNet [52] to extract high-resolution high-level features. DT-SCN [51] introduces a dual attention module (DAM) for more comprehensive Feature-level fusion which

TABLE I  
THE QUANTITATIVE EXPERIMENTAL RESULTS (%) ON THE CDD. THE VALUES IN BOLD ARE THE BEST

Method	Recall	Precision	OA	F1	Iou
FC-SC	71.10	78.62	94.55	74.67	58.87
SNUNet	80.29	84.52	95.73	82.35	69.91
DT-SCN	89.54	92.76	97.95	91.12	83.59
BIT	90.75	86.38	97.13	88.51	79.30
ChangeFormer	93.64	94.54	98.45	94.09	88.94
Proposed CADM	<b>95.10</b>	94.76	<b>98.87</b>	<b>94.93</b>	<b>90.56</b>

TABLE II  
THE QUANTITATIVE EXPERIMENTAL RESULTS (%) ON THE WHU. THE VALUES IN BOLD ARE THE BEST

Method	Recall	Precision	OA	F1	Iou
FC-SC	86.54	72.03	98.42	78.62	64.37
SNUNet	81.33	85.66	98.68	83.44	71.39
DT-SCN	93.60	88.05	99.32	90.74	83.55
BIT	87.94	89.98	99.30	88.95	81.53
ChangeFormer	86.43	89.69	98.95	88.03	78.46
Proposed CADM	<b>92.29</b>	<b>92.79</b>	<b>99.39</b>	<b>92.54</b>	<b>86.52</b>

exploits the interdependencies between channels and spatial positions, which improves the feature representation. BIT [41] incorporates transformers into the CD task to more effectively model the context present in bitemporal images. This approach facilitates the identification of changes of interest while excluding irrelevant alterations. Furthermore, ChangeFormer [42] utilize a hierarchical transformer encoder in a Siamese architecture with a simple MLP decoder, which method outperforms several other recent CD methods that employ very large ConvNets like ResNet18 and U-Net as the backbone.

### E. Experiment on CD DataSet (CDD)

TABLE III  
THE QUANTITATIVE EXPERIMENTAL RESULTS (%) ON THE LEVIR. THE VALUES IN BOLD ARE THE BEST

Method	Recall	Precision	OA	F1	Iou
FC-SC	77.29	89.04	98.25	82.75	69.95
SNUNet	84.33	88.55	98.70	86.39	76.11
DT-SCN	87.03	85.33	98.65	86.17	75.09
BIT	87.85	90.26	98.83	89.04	80.12
ChangeFormer	87.73	89.39	98.81	88.56	79.34
Proposed CADM	<b>91.24</b>	90.68	<b>99.14</b>	<b>90.96</b>	<b>83.56</b>

TABLE IV  
THE QUANTITATIVE EXPERIMENTAL RESULTS (%) ON THE GVL. THE VALUES IN BOLD ARE THE BEST

Method	Recall	Precision	OA	F1	Iou
FC-SC	89.53	74.47	96.47	81.31	67.24
SNUNet	91.67	87.22	98.97	89.39	80.85
DT-SCN	92.95	82.05	97.16	87.16	77.31
BIT	91.15	87.39	98.70	89.23	83.76
ChangeFormer	89.28	91.98	98.92	90.61	84.10
Proposed CADM	<b>94.25</b>	<b>93.79</b>	<b>99.32</b>	<b>94.02</b>	<b>89.09</b>

1) *Qualitative Evaluation:* The CD Dataset focuses on season-varying remote sensing image changes which are specifically designed to challenge CD algorithms by incorporating images acquired during different seasons, which exhibit distinct spectral characteristics.

As shown in Fig. 3 (a) – (b) which includes different types of land cover and land use types, such as urban areas, and agricultural fields during various seasons. This diversity enables the evaluation of CD algorithms across different spectral characteristics and different scenarios. 3 (c) – (i) illustrates the predictive capabilities of RSDiff and the compared methods.

Furthermore, the seasonal changes in vegetation and other land cover types can lead to areas of pseudo-changes in the CD maps as shown in Fig. 3. This makes it more challenging for algorithms to distinguish between actual changes and those caused by seasonal variability. The proposed RSDiff exhibits obvious advantages over its competitors in maintaining the details of the predicted change map and preserving the actual boundaries of changed objects.

Consequently, the change maps generated by RSDiff are closer to the ground truths than those of the other methods.

2) *Quantitative Evaluation*: We carry out experiments on the CD dataset to evaluate the effectiveness of RS-CADM, achieving the best experimental performance among all methods on the CDD dataset in terms of all evaluation indices with the highest OA, F1-score, precise, and IoU values, as shown in Table I. Although DDPM-CD achieved a slightly higher precision (95.05) than the proposed CADM (94.76), it generated more false negatives (FN), which subsequently led to a moderately lower recall compared to CADM. In contrast, CADM demonstrated a high recall while clearly outperforming the other methods in terms of precision.

#### F. Experiment on WHU Building CD Data Set

1) *Qualitative Evaluation*: We also conduct experiments on the WHU building change detection data set. The WHU dataset primarily focuses on urban changes, capturing various types of alterations such as construction, demolition, and land cover transformations. This dataset provides a challenging environment for CD algorithms, as it encompasses diverse land cover types, complex urban structures, and a wide range of spectral and spatial characteristics. To evaluate the performance of the proposed method on the WHU dataset, we conducted a series of comparative experiments with several state-of-the-art algorithms.

Visualizations of the CD results are depicted in Figs. 4. As can be seen from the figures, the WHU dataset contains intricate urban structures and diverse land cover types, which may lead to pseudo-changes and misclassifications in the CD maps of the compared methods. For instance, in the case of the FC-SC [13], DTCD [51], and SNUNet [15] results, there are notable omissions and false alarms in various urban objects, as shown in 4 (c) – (h). On the other hand, our proposed method effectively mitigates the influence of noise and pseudo-changes while preserving the internal compactness of urban objects.

2) *Quantitative Evaluation*: Quantitative results of the experiments are presented in Table II, which demonstrate the effectiveness of our method in handling the complexity of the WHU dataset. Our method achieves superior performance in terms of the F1 score, OA, and IoU metrics compared to other benchmark methods, indicating its ability to accurately detect urban changes.

#### G. Evaluation on LEVIR-CD Dataset

1) *Qualitative Evaluation*: Our experiments were conducted on the LEVIR-CD dataset, which is designed to detect building changes at various scales. The proposed CADM model was tested on dense, large-and-sparse, and small building targets, as shown in Fig. 5. However, the spectral variability caused by seasonal and illumination changes in the bitemporal images leads to areas of pseudo-changes in the CD maps of all compared methods. FC-SC [36], SNUNet, and other state-of-the-art methods' results showed edge blurring and lower internal compactness, as shown in Fig. 5 (c) – (h). In contrast, the proposed RSDiff can reduce noise and preserve the internal compactness of building objects, as shown in Fig. 5 (i). In addition, Fig. 5 displays the CD results for small building targets. In the CD maps of the compared methods, there are many pseudo-changes introduced by spectral changes in the building roofs and different imaging conditions. In addition, many small building targets are ignored. In comparison, the proposed RSDiff can accurately detect most of the small changed targets while suppressing pseudo-changes by focusing on the informative parts of features to enhance the separability between the changed and unchanged classes.

2) *Quantitative Evaluation*: CADM achieves the best experimental performance among all methods on the GVLM dataset, as shown in Table III, in terms of all evaluation indices, including the highest OA, F1-score, and IoU values. Although DDPM-CD achieved a slightly higher precision (91.39) than the proposed CADM (91.24), it generated a large number of false negatives (FN), which subsequently led to a moderately lower recall compared to CADM. In contrast, CADM demonstrated a high recall while clearly outperforming the other methods in terms of precision.

#### H. Experiments on the GVLM Dataset

1) *Qualitative Evaluation*: The GVLM dataset aims to detect landslide areas from bitemporal images by quantifying land cover changes. It consists of various types of landslides with irregular shapes occurring in regions with different land cover conditions and topographic heterogeneity as illustrated in Fig. 6 presents the comparison of CADM with other methods in generating CD maps. The change maps generated by the compared methods contain salt-and-pepper noise, leading to false alarms and omissions, especially at the boundaries of irregularly shaped landslide objects, as shown in Fig. 6(c) – (h). In contrast, CADM preserves the details of landslide objects and their boundaries while being more robust to noise. Therefore, the change maps generated by CADM are closer to the ground truth than those of the other methods, as shown in 6(i).

2) *Quantitative Evaluation*: CADM achieves the best experimental performance among all methods on the GVLM dataset, as shown in IV, in terms of the three most valuable evaluation indices, the highest OA, F1-score, and IoU values.

#### I. Visualization Via Gradient-Based Localization

To illuminate the performance enhancements achieved by our CADM, we utilized Grad-CAM [46] to visually examine

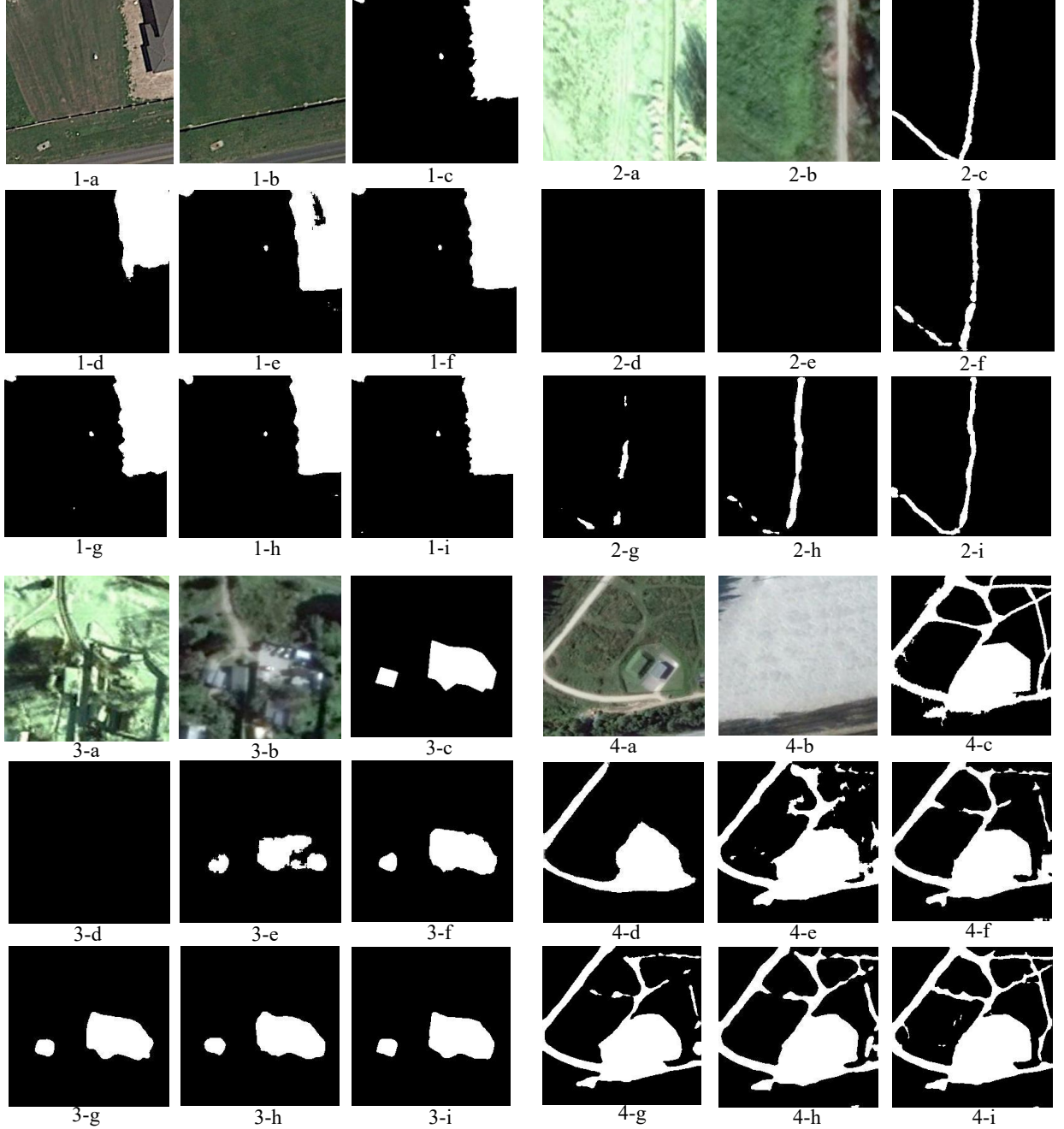


Fig. 3. Comparision of different state-of-the-art CD methods on CDD dataset: (a) Pre-change image, (b) Post-change image, (c) FC-SC, (d) SNUNet, (e) DT-SCN, (f) BIT, (g) ChangeFormer, (h) DDPM-CD, (i) CADM (ours), and (j) Ground-truth.

the output feature map from each decoder layer. However, unlike image classification tasks that assign a single class label to each image, change detection of bitemporal images involves labeling pixels individually. To cater to this difference, we modified the Grad-CAM approach [53] for change detection purposes, enabling visualization of classification decisions made by our CADM for individual pixels. In particular, the GradCAM discovers essential locations of the feature map for the final decision by tracking the gradient information flow. Consequently, class-discriminative locations in the Grad-CAM maps can show higher scores.

To showcase the effectiveness of our CADM in capturing

detailed difference information, we use Grad-CAM to visually compare the heatmaps generated by the localization decoder module with DDPM-CD, ChangeFormer and FC-SC. In Fig. 7, the first row of images displays the pre-change image, post-change image and the ground truth, respectively. Fig. 11(a),(b),(c) and (d) (i.e., the first, second, third, and forth rows) present the heatmaps of different levels produced by the DDPM-CD, ChangeFormer, FC-SC and our proposed method's decoders when attempting to classify each pixel as change region or not. For reference, a black dot is marked on the change region in the urban. It is important to note that brighter pixels have higher scores and are more likely to be

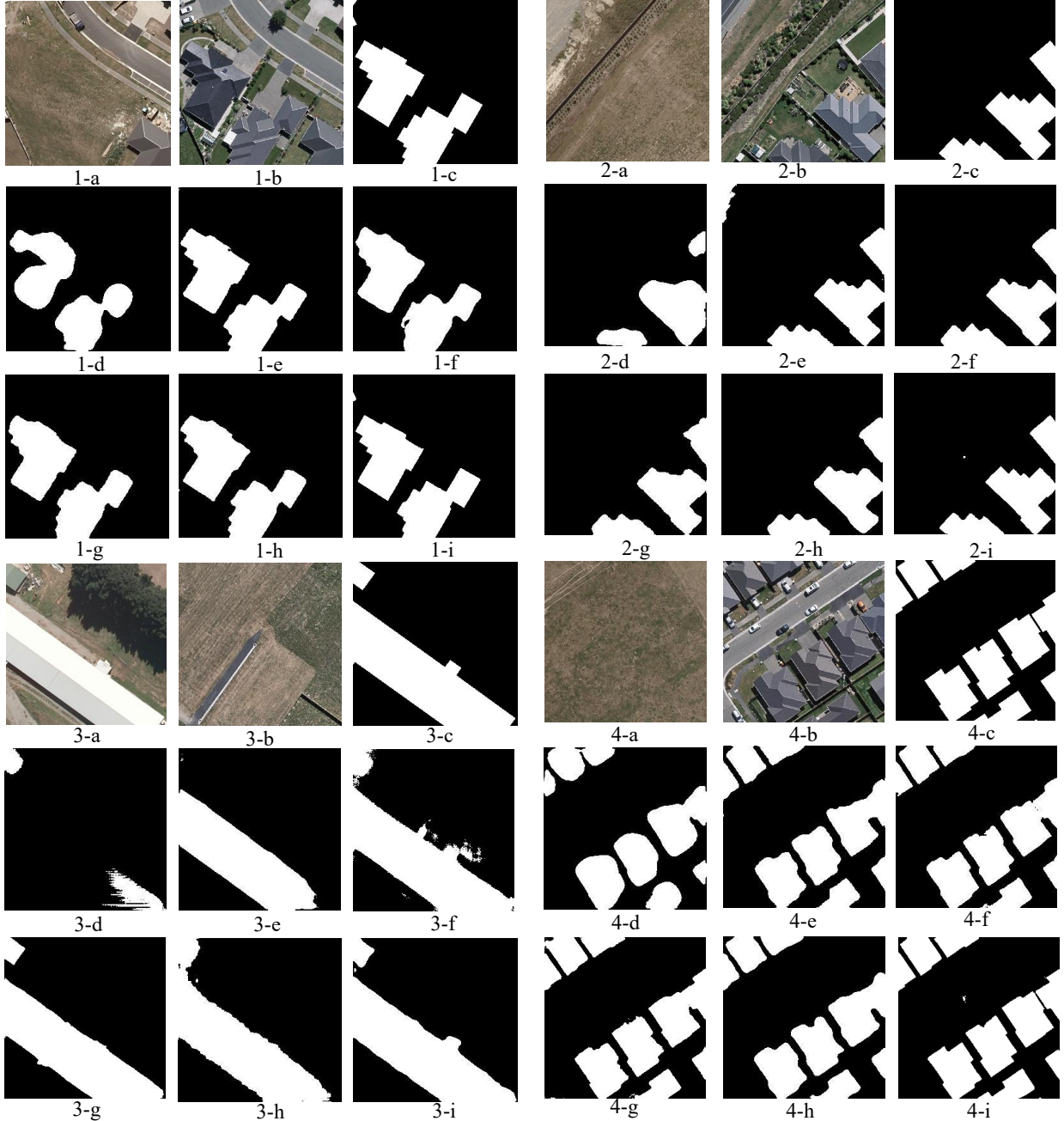


Fig. 4. Comparision of different state-of-the-art CD methods on WHU dataset: (a) Pre-change image, (b) Post-change image, (c) FC-SC, (d) SNUNet, (e) DT-SCN, (f) BIT, (g) ChangeFormer, (h) DDPM-CD, (i) CADM (ours), and (j) Ground-truth.

classified as change regions.

It can be observed that the feature maps generated by the conventional transformer (ChangeFormer) and CNN-based (FC-SC, DDPM-CD) methods are not sufficiently representative of the recognition of changed region, particularly for high-resolution shallow features that retain fine-grained details but lack semantic information. Despite the use of attention-augmented feature maps, multilevel self-attention (SA) modules still struggle to achieve adequate recalibration. In contrast, our proposed CADM generates more discriminative and change-aware feature maps at all levels, owing to the integration of multihead attention at various levels. Moreover,

our method enhances the representation and discrimination capabilities of shallow features while preserving rich local structures. As a result, the DDPM-based approach is capable of handling changed ground objects at different scales more effectively than its transformer and CNN-based counterparts.

#### J. Ablation Study

To validate the effectiveness of multi-scale Difference Conditional Encoding Information in change detection, we conducted two sets of ablation experiments, comparing them with our original model. In our current model, the difference feature maps of three scales (FEA1, the smallest scale; FEA2,

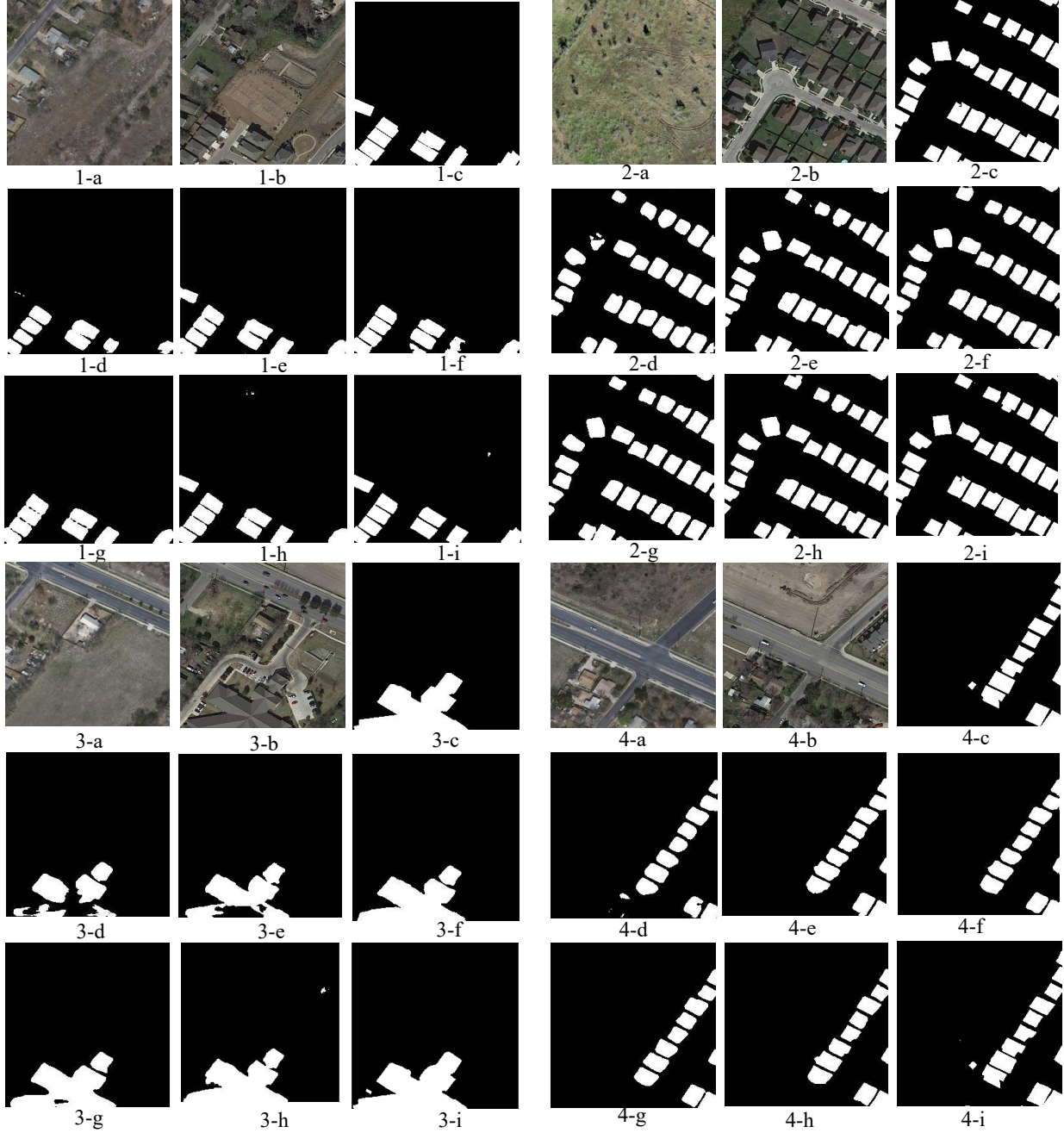


Fig. 5. Comparision of different state-of-the-art CD methods on LEVIR dataset: (a) Pre-change image, (b) Post-change image, (c) FC-SC, (d) SNUNet, (e) DT-SCN, (f) BIT, (g) ChangeFormer, (h) DDPM-CD, (i) CADM (ours), and (j) Ground-truth.

TABLE V  
ABLATION EXPERIMENT RESULTS(%) ON THE WHU DATASET.THE  
VALUES IN BOLD ARE THE BEST

SCALE1	SCALE2	SCALE3	OA	F1	IoU
		✓	99.32	91.32	84.35
	✓	✓	99.37	92.18	85.93
✓	✓	✓	<b>99.39</b>	<b>92.54</b>	<b>86.52</b>
✓	✓	✓	99.33	91.52	84.69

the medium scale; and FEA3, the largest scale) from the Difference Conditional Encoder are respectively conveyed to

the last encoding stage and Segmentation Decoder.

In the first ablation experiment, we employed the difference information from the medium scale (F2) and the smallest scale (F3). In the second ablation experiment, we directly fed the information from the smallest scale (F3) into the last encoding stage. These two experimental setups were designed to investigate the importance of multi-scale Difference Conditional Encoding Information for change detection performance.

As shown in the first three rows of the table V, the results of the ablation experiments reveal that the performance of the original model outperforms the other two ablated models, indicating that the multi-scale Difference Conditional Encod-

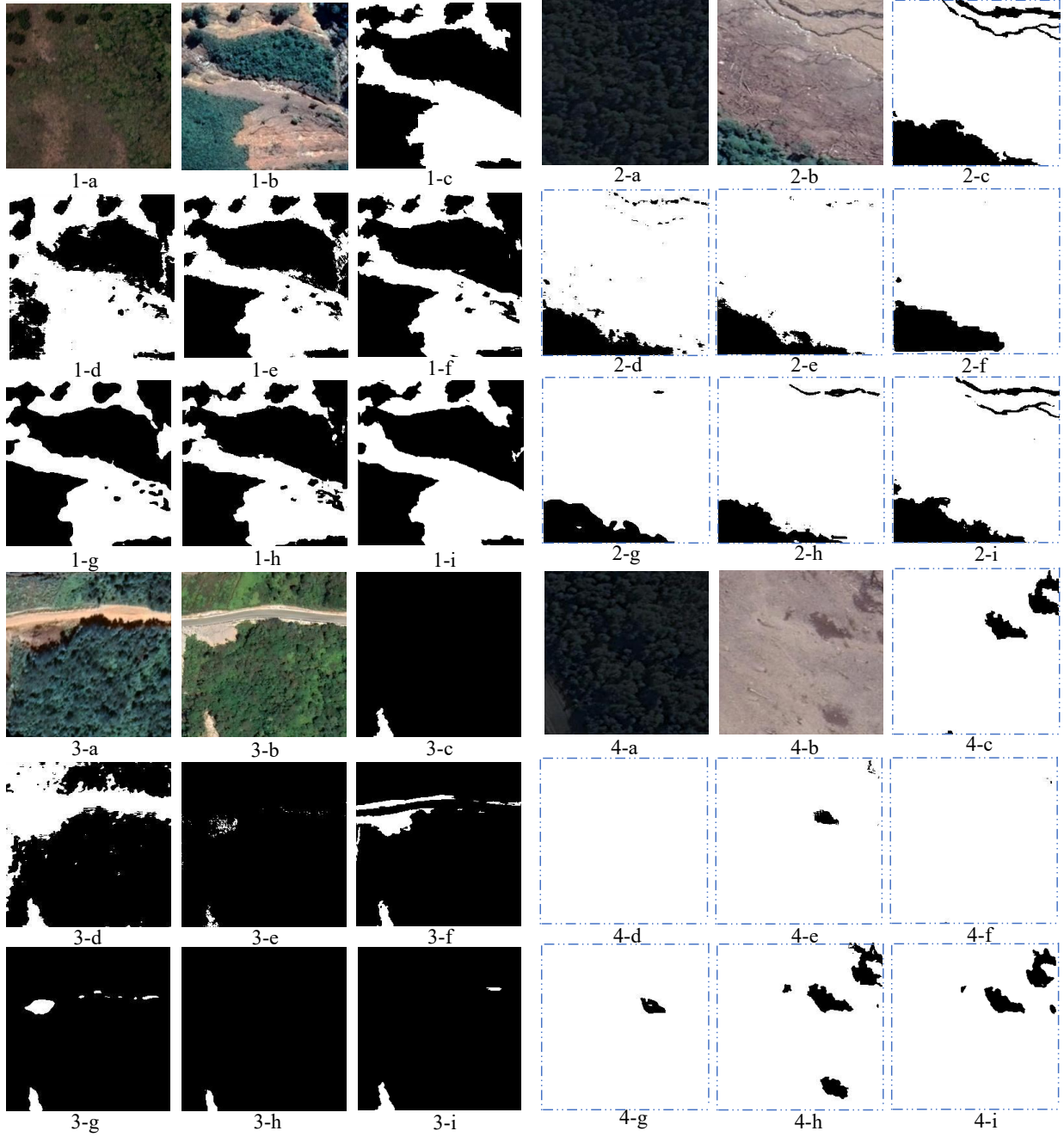


Fig. 6. Comparision of different state-of-the-art CD methods on GVLM dataset: (a) Pre-change image, (b) Post-change image, (c) FC-SC, (d) SNUNet, (e) DT-SCN, (f) BIT, (g) ChangeFormer, (h) DDPM-CD, (i) CADM (ours), and (j) Ground-truth.

ing Information plays a crucial role in enhancing the change detection results. In particular, the experiment with only the smallest scale information (F3) input to the last encoding stage demonstrates the importance of incorporating medium scale (F2) information. This further validates our hypothesis that multi-scale Difference Conditional Encoding Information contributes significantly to the change detection performance. Overall, these ablation studies corroborate the effectiveness of each component in our model and the necessity of utilizing multi-scale information for change detection.

Additionally, in order to validate the effectiveness of the noise suppression module (NSSE) incorporated into the feature

integration pathways, we conducted an ablation study by removing the NSSE module from our model. As shown in the last two rows of the table, the OA, F1, and IoU metrics correspond to the complete CADM model and the model with NSSE removed, respectively. The results of the ablation study demonstrated a notable decline in performance metrics when the NSSE module was removed. Specifically, the F1-score experienced a decrease of 1.02%, while the Intersection over Union (IoU) dropped by 1.83%. These findings highlight the crucial role played by the NSSE module in enhancing the model's performance in change detection tasks. The significant reduction in performance metrics observed in the ablation

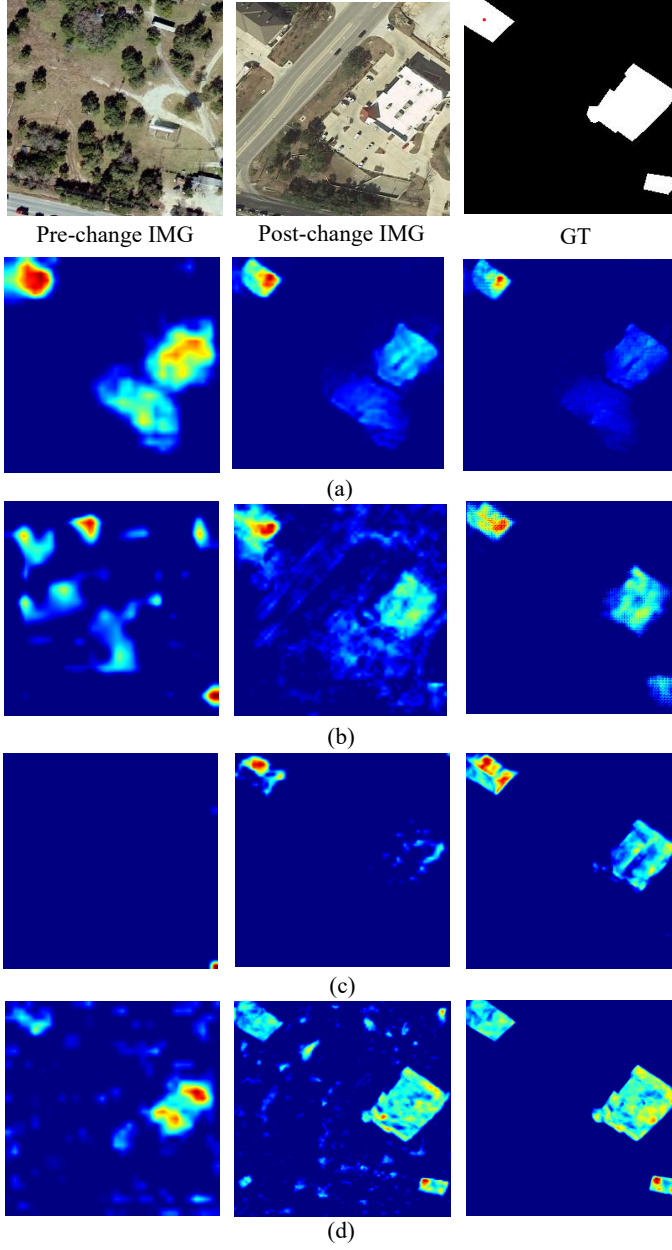


Fig. 7. In the heatmaps, (a), (b), (c), and (d) respectively represent the multi-scale feature maps in the Decoder of FC-EF, ChangeFormer, DDPM-CD, and CADM methods. The three columns of the visualization results represent the heatmaps corresponding to the feature maps at the smallest, intermediate, and largest scales in the Decoder, respectively.

study underlines the importance of incorporating the noise suppression module in the proposed framework to achieve superior change detection results.

#### K. General Analysis

In this paper, the integration of semantic segmentation functionality into the diffusion model was accomplished, and through a series of operations, including difference computation, decoding, and skip connections, CD maps were generated. It is worth mentioning that our semantic segmentation module and the diffusion model itself can be extensively applied to a wide range of scenarios beyond the realm of remote

sensing. These scenarios include medical-related datasets, and indoor and outdoor camera-captured datasets, among others.

By leveraging the versatility of our proposed method, we can potentially address various challenges and tasks associated with different types of datasets. In medical imaging, our approach could be employed for tasks such as tumor segmentation or anatomical structure identification. For indoor and outdoor camera-captured datasets, our method could be utilized for scene understanding, object tracking, or anomaly detection.

The adaptability and scalability of our approach make it a valuable tool for researchers and practitioners working in diverse fields, allowing them to build on our work and further explore its potential applications and improvements.

## V. CONCLUSION

In this paper, we propose an end-to-end DDPM-based model for CD in remote sensing images. The proposed novel remote sensing CD method, RS-CADM, significantly outperforms previous approaches by generating high-quality CD maps directly through end-to-end training which eliminates the need for additional pretraining of diffusion models. Moreover, RS-CADM introduces a creative encoding approach called Difference Conditional Encoding that provides change information for each sampling of the diffusion model. It effectively discriminates change information between pre-change and post-change images by integrating the current-step CD map's information with the extracted multi-level information from the conditional encoder. Attention mechanisms are employed to accomplish this fusion process, and the change information is computed through a pixel-wise difference operation. The strategy enables RS-CADM to dynamically localize and fine-tune the segmentation while addressing the issue of high-frequency noise information incorporation. Consequently, RS-CADM stands as a promising method for remote sensing CD, overcoming the limitations of previous approaches and delivering superior performance.

There are many challenges worthy of exploring in our future work. (1) we plan to integrate the Merge Temporal Features (MTF) module into our CADM model to further enhance its performance. The MTF module, consisting of five branches, effectively models different change types by utilizing minus operations and raw features to provide basic semantic information about objects. (2) Unet change to the transformer; For our second future work direction, we plan to replace the U-Net architecture in CADM with a Transformer-based model. Transformers have shown remarkable success in various computer vision tasks, and their ability to capture long-range dependencies and rich contextual information can potentially improve the performance of our CD model. (3) Multi-scale Fusion; As a third direction for future work, we plan to incorporate a multi-scale fusion strategy into our CADM model. Multi-scale fusion has been demonstrated to effectively capture both local and global contextual information at various scales, leading to a more comprehensive understanding of the scene.

## REFERENCES

[1] D. Lu, P. Mausel, E. Brondizio, and E. Moran, "Change detection techniques," *International journal of remote sensing*, vol. 25, no. 12, pp. 2365–2401, 2004.

[2] J.-F. Mas, "Monitoring land-cover changes: a comparison of change detection techniques," *International journal of remote sensing*, vol. 20, no. 1, pp. 139–152, 1999.

[3] M. Hussain, D. Chen, A. Cheng, H. Wei, and D. Stanley, "Change detection from remotely sensed images: From pixel-based to object-based approaches," *ISPRS Journal of photogrammetry and remote sensing*, vol. 80, pp. 91–106, 2013.

[4] P. Rosin, "Thresholding for change detection," in *Sixth International Conference on Computer Vision (IEEE Cat. No. 98CH36271)*. IEEE, 1998, pp. 274–279.

[5] W. A. Malila, "Change vector analysis: An approach for detecting forest changes with landsat," in *LARS symposia*, 1980, p. 385.

[6] F. Bovolo and L. Bruzzone, "A theoretical framework for unsupervised change detection based on change vector analysis in the polar domain," *IEEE Transactions on Geoscience and Remote Sensing*, vol. 45, no. 1, pp. 218–236, 2006.

[7] T. Celik, "Unsupervised change detection in satellite images using principal component analysis and  $k$ -means clustering," *IEEE geoscience and remote sensing letters*, vol. 6, no. 4, pp. 772–776, 2009.

[8] Z. Y. Lv, T. F. Liu, P. Zhang, J. A. Benediktsson, T. Lei, and X. Zhang, "Novel adaptive histogram trend similarity approach for land cover change detection by using bitemporal very-high-resolution remote sensing images," *IEEE Transactions on Geoscience and Remote Sensing*, vol. 57, no. 12, pp. 9554–9574, 2019.

[9] M. Zhang and W. Shi, "A feature difference convolutional neural network-based change detection method," *IEEE TRANSACTIONS ON GEOSCIENCE AND REMOTE SENSING*, vol. 58, no. 10, pp. 7232–7246, OCT 2020.

[10] S. Ji, S. Wei, and M. Lu, "Fully convolutional networks for multisource building extraction from an open aerial and satellite imagery data set," *IEEE TRANSACTIONS ON GEOSCIENCE AND REMOTE SENSING*, vol. 57, no. 1, pp. 574–586, JAN 2019.

[11] B. Hou, Q. Liu, H. Wang, and Y. Wang, "From w-net to cdgan: Bitemporal change detection via deep learning techniques," *IEEE TRANSACTIONS ON GEOSCIENCE AND REMOTE SENSING*, vol. 58, no. 3, pp. 1790–1802, MAR 2020.

[12] M. Yang, L. Jiao, F. Liu, B. Hou, and S. Yang, "Transferred deep learning-based change detection in remote sensing images," *IEEE TRANSACTIONS ON GEOSCIENCE AND REMOTE SENSING*, vol. 57, no. 9, pp. 6960–6973, SEP 2019.

[13] Y. Zhan, K. Fu, M. Yan, X. Sun, H. Wang, and X. Qiu, "Change detection based on deep siamese convolutional network for optical aerial images," *IEEE Geoscience and Remote Sensing Letters*, vol. 14, no. 10, pp. 1845–1849, 2017.

[14] R. C. Daudt, B. Le Saux, and A. Boulch, "Fully convolutional siamese networks for change detection," in *2018 25th IEEE International Conference on Image Processing (ICIP)*. IEEE, 2018, pp. 4063–4067.

[15] S. Fang, K. Li, J. Shao, and Z. Li, "Snnunet-cd: A densely connected siamese network for change detection of vhr images," *IEEE Geoscience and Remote Sensing Letters*, vol. 19, pp. 1–5, 2022.

[16] C. Zhang, P. Yue, D. Tapete, L. Jiang, B. Shangguan, L. Huang, and G. Liu, "A deeply supervised image fusion network for change detection in high resolution bi-temporal remote sensing images," *ISPRS JOURNAL OF PHOTOGRAVIMETRY AND REMOTE SENSING*, vol. 166, pp. 183–200, AUG 2020.

[17] Q. Shi, M. Liu, S. Li, X. Liu, F. Wang, and L. Zhang, "A deeply supervised attention metric-based network and an open aerial image dataset for remote sensing change detection," *IEEE TRANSACTIONS ON GEOSCIENCE AND REMOTE SENSING*, vol. 60, 2022.

[18] Q. Zhu, X. Guo, W. Deng, S. Shi, Q. Guan, Y. Zhong, L. Zhang, and D. Li, "Land-use/land-cover change detection based on a siamese global learning framework for high spatial resolution remote sensing imagery," *ISPRS JOURNAL OF PHOTOGRAVIMETRY AND REMOTE SENSING*, vol. 184, pp. 63–78, FEB 2022.

[19] X. Zhang, W. Yu, and M.-O. Pun, "Multilevel deformable attention-aggregated networks for change detection in bitemporal remote sensing imagery," *IEEE Transactions on Geoscience and Remote Sensing*, vol. 60, pp. 1–18, 2022.

[20] H. Chen and Z. Shi, "A spatial-temporal attention-based method and a new dataset for remote sensing image change detection," *Remote Sensing*, vol. 12, no. 10, 2020. [Online]. Available: <https://www.mdpi.com/2072-4292/12/10/1662>

[21] —, "A spatial-temporal attention-based method and a new dataset for remote sensing image change detection," *Remote Sensing*, vol. 12, no. 10, 2020. [Online]. Available: <https://www.mdpi.com/2072-4292/12/10/1662>

[22] Z. Zheng, Y. Zhong, S. Tian, A. Ma, and L. Zhang, "Changemask: Deep multi-task encoder-transformer-decoder architecture for semantic change detection," *ISPRS JOURNAL OF PHOTOGRAVIMETRY AND REMOTE SENSING*, vol. 183, pp. 228–239, JAN 2022.

[23] X. Xu, J. Li, and Z. Chen, "Tcianet: Transformer-based context information aggregation network for remote sensing image change detection," *IEEE JOURNAL OF SELECTED TOPICS IN APPLIED EARTH OBSERVATIONS AND REMOTE SENSING*, vol. 16, pp. 1951–1971, 2023.

[24] Z. Zheng, Y. Zhong, S. Tian, A. Ma, and L. Zhang, "Changemask: Deep multi-task encoder-transformer-decoder architecture for semantic change detection," *ISPRS JOURNAL OF PHOTOGRAVIMETRY AND REMOTE SENSING*, vol. 183, pp. 228–239, JAN 2022.

[25] X. Zhang, W. Yu, M.-O. Pun, and M. Liu, "Style transformation-based change detection using adversarial learning with object boundary constraints," in *2021 IEEE International Geoscience and Remote Sensing Symposium (IGARSS)*. IEEE, 2021, pp. 3117–3120.

[26] H. Li, Y. Yang, M. Chang, S. Chen, H. Feng, Z. Xu, Q. Li, and Y. Chen, "Srdiff: Single image super-resolution with diffusion probabilistic models," *Neurocomputing*, vol. 479, pp. 47–59, 2022.

[27] J. Wu, H. Fang, Y. Zhang, Y. Yang, and Y. Xu, "Medsegdiff: Medical image segmentation with diffusion probabilistic model," *arXiv preprint arXiv:2211.00611*, 2022.

[28] J. Wu, R. Fu, H. Fang, Y. Zhang, and Y. Xu, "Medsegdiff-v2: Diffusion based medical image segmentation with transformer," *arXiv preprint arXiv:2301.11798*, 2023.

[29] D. Baranchuk, I. Rubachev, A. Voynov, V. Khrulkov, and A. Babenko, "Label-efficient semantic segmentation with diffusion models," *arXiv preprint arXiv:2112.03126*, 2021.

[30] R. Rombach, A. Blattmann, D. Lorenz, P. Esser, and B. Ommer, "High-resolution image synthesis with latent diffusion models," in *Proceedings of the IEEE/CVF Conference on Computer Vision and Pattern Recognition*, 2022, pp. 10684–10695.

[31] J. Ho, C. Saharia, W. Chan, D. J. Fleet, M. Norouzi, and T. Salimans, "Cascaded diffusion models for high fidelity image generation," *J. Mach. Learn. Res.*, vol. 23, no. 47, pp. 1–33, 2022.

[32] A. Ramesh, P. Dhariwal, A. Nichol, C. Chu, and M. Chen, "Hierarchical text-conditional image generation with clip latents," *arXiv preprint arXiv:2204.06125*, 2022.

[33] J. Ho, A. Jain, and P. Abbeel, "Denoising diffusion probabilistic models," *Advances in Neural Information Processing Systems*, vol. 33, pp. 6840–6851, 2020.

[34] W. G. C. Bandara, N. G. Nair, and V. M. Patel, "Ddpmd-cd: Remote sensing change detection using denoising diffusion

probabilistic models,” *arXiv preprint arXiv:2206.11892*, 2022.

[35] T. Salimans, D. Kingma, and M. Welling, “Markov chain monte carlo and variational inference: Bridging the gap,” in *International conference on machine learning*. PMLR, 2015, pp. 1218–1226.

[36] M. Zhang, G. Xu, K. Chen, M. Yan, and X. Sun, “Triplet-based semantic relation learning for aerial remote sensing image change detection,” *IEEE Geoscience and Remote Sensing Letters*, vol. 16, no. 2, pp. 266–270, 2018.

[37] M. Wang, K. Tan, X. Jia, X. Wang, and Y. Chen, “A deep siamese network with hybrid convolutional feature extraction module for change detection based on multi-sensor remote sensing images,” *Remote Sensing*, vol. 12, no. 2, p. 205, 2020.

[38] R. C. Daudt, B. Le Saux, and A. Boulch, “Fully convolutional siamese networks for change detection,” in *2018 25th IEEE International Conference on Image Processing (ICIP)*. IEEE, 2018, pp. 4063–4067.

[39] J. Liu, M. Gong, K. Qin, and P. Zhang, “A deep convolutional coupling network for change detection based on heterogeneous optical and radar images,” *IEEE transactions on neural networks and learning systems*, vol. 29, no. 3, pp. 545–559, 2016.

[40] L. Mou, L. Bruzzone, and X. X. Zhu, “Learning spectral-spatial-temporal features via a recurrent convolutional neural network for change detection in multispectral imagery,” *IEEE Transactions on Geoscience and Remote Sensing*, vol. 57, no. 2, pp. 924–935, 2018.

[41] H. Chen, Z. Qi, and Z. Shi, “Remote sensing image change detection with transformers,” *IEEE Transactions on Geoscience and Remote Sensing*, vol. 60, pp. 1–14, 2021.

[42] W. G. C. Bandara and V. M. Patel, “A transformer-based siamese network for change detection,” in *IGARSS 2022-2022 IEEE International Geoscience and Remote Sensing Symposium*. IEEE, 2022, pp. 207–210.

[43] C. Zhang, L. Wang, S. Cheng, and Y. Li, “Swinsunet: Pure transformer network for remote sensing image change detection,” *IEEE Transactions on Geoscience and Remote Sensing*, vol. 60, pp. 1–13, 2022.

[44] H. Chen and Z. Shi, “A spatial-temporal attention-based method and a new dataset for remote sensing image change detection,” *Remote Sensing*, vol. 12, no. 10, p. 1662, 2020.

[45] I. Pitas, *Digital image processing algorithms and applications*. John Wiley & Sons, 2000.

[46] “Digital image processing algorithms and applications. i[book review],” *IEEE Signal Processing Magazine*, vol. 18, no. 2, pp. 58–58, 2001.

[47] M. Lebedev, Y. V. Vizilter, O. Vygolov, V. Knyaz, and A. Y. Rubis, “Change detection in remote sensing images using conditional adversarial networks,” *International Archives of the Photogrammetry, Remote Sensing & Spatial Information Sciences*, vol. 42, no. 2, 2018.

[48] H. Chen and Z. Shi, “A spatial-temporal attention-based method and a new dataset for remote sensing image change detection,” *Remote Sensing*, vol. 12, no. 10, 2020. [Online]. Available: <https://www.mdpi.com/2072-4292/12/10/1662>

[49] W. G. C. Bandara and V. M. Patel, “Revisiting consistency regularization for semi-supervised change detection in remote sensing images,” 2022.

[50] X. Zhang, W. Yu, M.-O. Pun, and W. Shi, “Cross-domain landslide mapping from large-scale remote sensing images using prototype-guided domain-aware progressive representation learning,” *ISPRS Journal of Photogrammetry and Remote Sensing*, vol. 197, pp. 1–17, 2023.

[51] Y. Liu, C. Pang, Z. Zhan, X. Zhang, and X. Yang, “Building change detection for remote sensing images using a dual-task constrained deep siamese convolutional network model,” *IEEE Geoscience and Remote Sensing Letters*, vol. 18, no. 5, pp. 811–815, 2020.

[52] Z. Zhou, M. M. Rahman Siddiquee, N. Tajbakhsh, and J. Liang, “Unet++: A nested u-net architecture for medical image segmentation,” in *Deep Learning in Medical Image Analysis and Multimodal Learning for Clinical Decision Support: 4th International Workshop, DLMIA 2018, and 8th International Workshop, ML-CDS 2018, Held in Conjunction with MICCAI 2018, Granada, Spain, September 20, 2018, Proceedings 4*. Springer, 2018, pp. 3–11.

[53] X. Ma, X. Zhang, and M.-O. Pun, “A crossmodal multiscale fusion network for semantic segmentation of remote sensing data,” *IEEE Journal of Selected Topics in Applied Earth Observations and Remote Sensing*, vol. 15, pp. 3463–3474, 2022.